Biomaterials 30 (2009) 5720–5728

Contents lists available at ScienceDirect

Biomaterials

journal homepage: www.elsevier.com/locate/biomaterials

Nanodiamond–insulin complexes as pH-dependent protein delivery vehicles

Rafael A. Shimkunas [a], Erik Robinson [a], Robert Lam [b], Steven Lu [a], Xiaoyang Xu [c], Xue-Qing Zhang [a], Houjin Huang [a,b], Eiji Osawa [d], Dean Ho [a,b,e,f,*]

[a] Department of Biomedical Engineering, Northwestern University, Evanston, IL 60208, USA
[b] Department of Mechanical Engineering, Northwestern University, Evanston, IL 60208, USA
[c] Department of Chemistry, Northwestern University, Evanston, IL 60208, USA
[d] NanoCarbon Research Institute, Ltd., Asama Research Extension Center, Shinshu University, 3-15-1 Tokita, Ueda, Nagano 386-8567, Japan
[e] Robert H. Lurie Comprehensive Cancer Center, Northwestern University, Chicago, IL 60611, USA
[f] Institute for Bionanotechnology in Medicine (IBNAM), Northwestern University, Chicago, IL 60611, USA

ARTICLE INFO

Article history:
Received 22 May 2009
Accepted 6 July 2009
Available online 26 July 2009

Keywords:
Nanodiamond
Insulin
Drug delivery
Wound healing
Nanomedicine

ABSTRACT

Enhanced specificity in drug delivery aims to improve upon systemic elution methods by locally concentrating therapeutic agents and reducing negative side effects. Due to their robust physical properties, biocompatibility and drug loading capabilities, nanodiamonds serve as drug delivery platforms that can be applied towards the elution of a broad range of therapeutically-active compounds. In this work, bovine insulin was non-covalently bound to detonated nanodiamonds via physical adsorption in an aqueous solution and demonstrated pH-dependent desorption in alkaline environments of sodium hydroxide. Insulin adsorption to NDs was confirmed by FT-IR spectroscopy and zeta potential measurements, while both adsorption and desorption were visualized with TEM imaging, quantified using protein detection assays and protein function demonstrated by MTT and RT-PCR. NDs combined with insulin at a 4:1 ratio showed 79.8 ± 4.3% adsorption and 31.3 ± 1.6% desorption in pH-neutral and alkaline solutions, respectively. Additionally, a 5-day desorption assay in NaOH (pH 10.5) and neutral solution resulted in 45.8 ± 3.8% and 2.2 ± 1.2% desorption, respectively. MTT viability assays and quantitative RT-PCR (expression of Ins1 and Csf3/G-csf genes) reveal bound insulin remains inactive until alkaline-mediated desorption. For applications in sustained drug delivery and therapy we have developed a therapeutic protein–ND complex with demonstrated tunable release and preserved activity.

1. Introduction

There remains a significant need for enhanced methods of drug delivery to maximize therapeutic effects while decreasing associated complications due to nonspecific or over-elution. Systemic treatments pose various problems concerning the pervasiveness of drug exposure to the body and can lead to harmful side effects outweighing treatment benefits. Effectively targeting and controlling drug delivery in an effort to limit nonspecific drug–tissue interaction is a desired outcome. In this regard, site-specific drug delivery is highly advantageous for a host of ailments ranging from cancer to cardiovascular treatments. Recent advances in nanomedicine (e.g., imaging and diagnosis [1–3], drug delivery [4–10] and gene therapy [11–13]) have demonstrated the benefits of nanoparticle therapeutics, including reduction of drug concentration, targeted delivery, diminished complications and biocompatibility [3,14–16].

The application of nanoparticles as effective drug delivery vehicles as well as in mechanical, electrical and MEMS applications has been demonstrated with carbon nanotubes, nanodiamonds, nanoparticle-embedded films, natural and synthetic polymers, lipid vesicles and a host of other nanoscale species [8,9,17–27]. With specific regard to the delivery of insulin, the model protein utilized in this study, a spectrum of nanomaterial-based vehicles has been explored for its delivery towards the treatment of physiological disorders such as diabetes. For example, *in vivo* studies with oral and transmucosal delivered insulin-loaded gold nanoparticles have led to promising initial results in reducing systemic glucose levels in diabetic rats [28]. Furthermore, implantable and integrated smart release drug delivery and sensor devices have been proposed for distribution of insulin *via* feedback-controlled systems. Within these instruments, fully programmable and independent systems capable of delivering the proper amount of drugs

* Corresponding author. Department of Biomedical Engineering, Northwestern University, 2145 Sheridan Road, Evanston, IL 60208, USA. Tel.: +1 847 467 0548; fax: +1 847 491 3915.
E-mail address: d-ho@northwestern.edu (D. Ho).

0142-9612/$ – see front matter © 2009 Elsevier Ltd. All rights reserved.
doi:10.1016/j.biomaterials.2009.07.004

at a suitable time were capable of mimicking naturally occurring biologically processes [29]. Poly(lactic-*co*-glycolic acid) (PLGA)-based shells with encapsulated insulin have also been explored for the sustained release of insulin and maintained blood glucose levels [30]. The oral delivery of dextran sulfate/chitosan-based nanoparticles has also been explored in diabetic rats to increase pharmacological availability [31]. Furthermore, hydrogels based on poly(methacrylic acid-grafted-ethylene glycol) and wheat germ agglutinin functionalized poly(methacrylic acid-grafted-ethylene glycol) have also been explored for the oral delivery of insulin with pH-dependent release characteristics [32].

Towards the development of a scalable delivery platform with facile drug functionalization capabilities, high surface area-to-volume ratios for enhanced loading parameters, innate bio-amenable properties due to their carbon composition, and a broad range of additional integrative benefits towards therapeutic delivery, detonation NDs are of particular interest for the delivery of protein-based therapeutics such as insulin. They have been validated as effective small molecule delivery vehicles with functionalized surfaces [9,33,34] and biocompatibility that has been verified at the genetic level [15,35–37]. These attributes create a dynamic interface where the interactions between the NDs and other particles or molecules can be defined by ND surface characteristics. An example of such an interaction is given by the NDs possessing hydrophilic hydroxyl and carboxylic functional groups owing to characteristic surface charges and allowing for dispersion in water [8,33,34]. The future prospects of developing NDs for biomedical applications and their suggested biocompatibility manifest the NDs as favorable carbon-based biomaterials.

Numerous studies have shown the efficacy of transiently linking or conjugating drugs and therapeutic molecules to the NDs, including chemotherapy agents, organic molecules and proteins [34,38,39]. There has been recent work addressing the drug release profiles of the NDs [8,9], yet there has been little scientific inquiry relating to the release of protein-based drugs using the NDs. Examples of protein-based drugs include cytokines, monoclonal antibodies, hormones and clotting factors, all of which hold great promise or have been substantiated as therapeutic agents.

In this study we have examined the hormone insulin as a model for protein desorption due to its relative stability and measurable response in cellular studies. The adsorption and desorption characteristics of insulin on nanodiamonds as a platform for protein-based drugs were investigated and confirmed via UV–vis spectrophotometry, transmission electron microscopy (TEM), and zeta potential measurement/dynamic light scattering (DLS). Furthermore, the confirmation of protein functionality was confirmed using the RAW 264.7 cell line for insulin-mediated cellular recovery MTT assays. In addition, the 3T3-L1 cell line was utilized for quantitative real-time polymerase chain reaction (RT-PCR) assays for insulin-induced upregulated Insulin 1 (Ins1) and Granulocyte colony-stimulating factor (Csf3/G-csf) gene expression, which are both readouts for cellular-insulin interactions.

2. Materials and methods

2.1. Cell culture

Murine cell lines including RAW 264.7 macrophages and 3T3-L1 fibroblasts (ATCC Manassas, VA) were maintained in DMEM (Cellgro, Herndon, VA) with 1% penicillin/streptomycin (Cambrex, East Rutherford, NJ) containing 10% FBS (ATCC) and 10% CBS (ATCC), respectively, at 37 °C in 5% CO_2. 3T3-L1 fibroblasts were cultured in DMEM supplemented with 10% CBS until they reached 90% confluency, whereupon adipocyte differentiation commenced in accordance to previously established protocols [40,41]. Media was replaced with DMEM, 10% FBS, 0.86 μM insulin, 0.25 μM dexamethasone and 0.5 mM isobutylmethylxanthine (IBMX) (Sigma Aldrich St. Louis, MO) for 4 days, and the media was renewed on day 2. Media was replaced on day 4 with DMEM, 10% FBS and 0.86 μM insulin, and again on day 6 with DMEM, 10% FBS for an additional 4 days. Cells were fully differentiated on day 10, and subsequently cultured in DMEM, 10% FBS and 1% penicillin/streptomycin.

2.2. Formation of ND–insulin complex

Nanodiamonds (NanoCarbon Research Institute Co., Ltd., Nagano, Japan) dispersed in water underwent ultrasonication for 4 h (100 W, VWR 150D Sonicator) to further disperse the ND aggregates. Aqueous insulin was then added to ND solutions at varying ratios and mixed thoroughly to promote insulin binding to the NDs by physical adsorption.

2.3. Protein characterization

FITC-labeled insulin (Sigma–Aldrich) was dissolved in a 1 mM stock solution. Samples were measured using a Beckman Coulter DU730 UV/vis spectrophotometer (Fullerton, CA) at peak absorbance of approximately 494 nm (peak varied with solvent). Bovine insulin (Sigma–Aldrich), dissolved in acetic acid (pH 3) and neutralized with 1 mM NaOH, was used to supplement the results from FITC insulin. Protein detection was performed using the Micro BCA Protein Assay Kit (Thermo Scientific, Rockford, IL), measuring absorbance at 562 nm.

2.4. FT-IR and TEM characterization

A 4:1 ratio of NDs to insulin was prepared, centrifuged at 14,000 rpm for 2 h and the supernatant was removed. The ND–insulin pellet was rinsed with water and dried under vacuum. Individual ND and insulin samples were also prepared by dehydrating each respective solution. Additionally, a sample of NaOH-treated ND–insulin was prepared for TEM imaging by adding 1 mM NaOH adjusted to pH 10.5 to ND–insulin, centrifuging for 2 h at 14,000 rpm and isolating the ND pellet. Samples were characterized at room temperature using a Thermo Nicolet Nexus 870 FT-IR spectrometer and a Hitachi H-8100 TEM (Pleasanton, CA).

2.5. DLS analysis

Hydrodynamic size and zeta potential of samples were measured with a Zetasizer Nano (Malvern Instruments, Worcestershire, United Kingdom). The NDs and insulin were prepared as previously described. Briefly, the particles were suspended in buffer with corresponding pH at a concentration of 50 mg/mL. The size measurements were performed at 25 °C and at a 173° scattering angle. The mean hydrodynamic diameter was determined by cumulative analysis. The zeta potential determinations were based on the electrophoretic mobility of the microparticles in the aqueous medium, which was performed using folded capillary cells in automatic mode.

2.6. Insulin adsorption and desorption

Determination of insulin adsorption to the NDs was performed by protein detection assays before and after centrifugation. Insulin was added to an ND suspension, centrifuged at 14,000 rpm for 2 h and the resultant solution was extracted and quantified. Detection of desorbed insulin was performed by adding alkaline solutions of 1 mM NaOH, adjusted for varying pH, to samples of ND–insulin in suspension. Similar methods were employed for binding ratio determination.

Additionally, a 5-day desorption test was conducted to determine cumulative insulin release. Samples were prepared by combining the NDs and insulin (4:1 ratio), centrifuging the sample at 14,000 rpm for 2 h and extracting the remaining solution to remove any non-adsorbed insulin. Subsequently, a 1 mM NaOH solution adjusted to pH 10.5 was added to the samples, mixed thoroughly, and centrifuged after a 24-hour period to determine protein concentration utilizing the BCA assay. In addition to alkaline-mediated release, water was added to a separate set of samples. The samples were replenished with NaOH or water after each measurement for the respective conditions, and the process was repeated every 24 h over the course of 5 days.

2.7. MTT cell viability assay

RAW 264.7 murine macrophages were plated in 96-well plates, serum-starved for 8 h and then incubated for 24 h. Post-starvation media consisted of the following conditions: DMEM, 0.1 μM insulin, 1 μM insulin, DMEM 10% FBS, approximately 0.1 μM insulin released from ND–insulin complex by NaOH at pH 10.5 (insulin present in media), resultant solution from centrifuged ND–insulin in water, ND–insulin treated with NaOH at pH 10.5 (1 μM total insulin, ND–insulin complex present in media) and ND–insulin (1 μM total insulin, ND–insulin complex present in media). Insulin released from the NDs was prepared by centrifuging samples of NDs with adsorbed insulin in NaOH and extracting the resultant solution, which could be reconstituted with media to 0.1 μM insulin. In a similar fashion, water was utilized as a neutral solution for relevant desorption analysis. Methylthiazolyldiphenyl-tetrazolium bromide (MTT) solution (Sigma–Aldrich) was added corresponding to 10% of the total volume, and then incubated for 3 h. After formazan crystal formation, the media was removed and the MTT solvent, 0.1 N HCl in anhydrous isopropanol (Sigma–Aldrich), was added to samples to solubilize the MTT dye. Sample

absorbance measurements occurred at 570 nm, accounting for background at a wavelength of 690 nm.

2.8. Quantitative RT-PCR

RT-PCR procedures were conducted as described previously [40]. 3T3-L1 adipocytes were plated in 6-well plates, serum-starved for 4 h and then recovered in media solutions of DMEM, 0.1 μM insulin, approximately 0.1 μM insulin released from ND–insulin by NaOH (pH 10.5), resultant solution from centrifuged ND–insulin in pH-neutral water, ND–insulin treated with NaOH (1 μM total insulin) and NDs with bound insulin (ND–insulin, 1 μM total insulin). Preparations of media solutions containing DMEM, insulin, NDs and NaOH were conducted in a similar fashion to those implemented for the MTT assay. RNA isolation was completed by lysing cells with TRIzol reagent (Invitrogen Corporation, Carlsbad, CA) followed by chloroform addition to obtain the genetic material by centrifugation. cDNA synthesis was performed using the iScript Select cDNA Synthesis Kit (Bio-Rad, Hercules, CA). PCR expression of the Ins1 and Csf3/G-csf genes (Integrated DNA Technologies, Coralville, IA) was quantified by the MyiQ Single Color Real-Time PCR machine (Bio-Rad, Hercules, CA) using SYBR Green detection reagents (Quanta Biosciences, Gaithersburg, MD). The Rpl32 gene (Integrated DNA Technologies) served as the housekeeping gene for normalization of cDNA among samples. The primer sequences for genes are given: Ins1, 5′-AGGTGGCCCGGCAGAAG-3′ and 5′-GCCTTAGTTGCAGTAGTTCTCCAGCT-3′; Csf3/G-csf, 5′-CCAGAGGCGCATGAAGCTAAT-3′ and 5′-CGGCCTCTCGTCCTGACCAT-3′; Rpl32, 5′-AACCGAAAAGCCATTGTAGAAA-3′ and 5′-CCTGGCGTTGGGATTGG-3′.

3. Results

3.1. FT-IR and TEM

Illustrated in Fig. 1 is a representation of the proposed mechanism of insulin adsorption and desorption in neutral and alkaline solutions, respectively. Transmission electron microscopy (TEM) images in Fig. 2 show bare NDs (a), NDs with adsorbed insulin (b) and the ND–insulin complex after treatment with NaOH (c). In (b) there is an apparent layer of material coating the NDs approximately 5–10 nm in thickness. The NaOH-treated ND–insulin sample (c) qualitatively shows a diminished layer of material on the NDs, suggesting NaOH treatment of ND–insulin removed the material present on the ND surface. Fourier transform infrared (FT-IR) spectroscopy (Fig. 3) suggests the presence of insulin on NDs. Samples of insulin (1), bare NDs (2) and ND-insulin (3) are shown, with spectrum peaks of ND–insulin complexes indicating characteristic peaks similar to insulin.

3.2. DLS analysis

The interaction between the NDs and insulin was characterized by means of dynamic light scattering (DLS) analysis, revealing the nanodiamond–insulin cluster sizes and polydispersity index information which are summarized in Table 1 while the zeta potential properties are further illustrated in Fig. 4. The average ND cluster size remained similar at pH levels of 7 and 10.5, whereas insulin aggregates showed a larger average size at pH 10.5. The ND–insulin complex demonstrated an average size comparable to bare NDs and a decreased polydispersity index. NDs exhibited a slightly positive zeta potential at both pH 7 and 10.5, while insulin and ND–insulin resulted in negative values. The zeta potential of insulin and ND–insulin at pH 10.5 was substantially more negative than similar samples at pH 7.

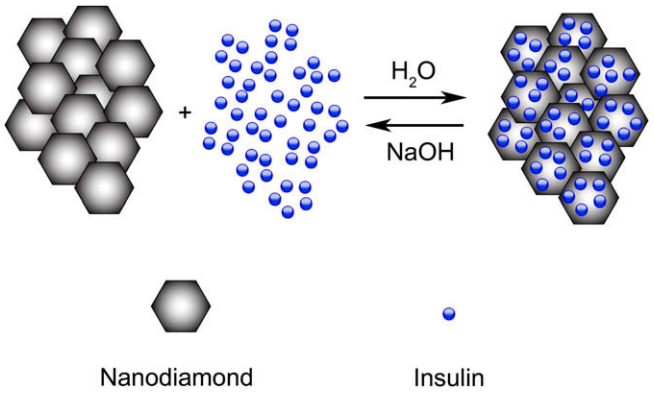

Fig. 1. A schematic illustration showing insulin adsorption to NDs in water and desorption in the presence of NaOH. Insulin non-covalently binds to the ND surface in water by means of electrostatic and other interactions. The shift to an alkaline environment alters the insulin surface charge characteristics, thereby causing release from the ND surface.

3.3. Adsorption

Fig. 1 shows a schematic of how insulin in neutral solutions will bind by physical adsorption to the NDs. FITC insulin samples of varying concentrations were mixed thoroughly with the NDs (100 μg/mL) to promote adsorption. The observed absorbance for ND–insulin (Fig. 5a) differs from that of aqueous insulin due to the adsorption of insulin to the NDs. The ND–insulin complex, however, retains the spectral characteristics necessary to quantify the presence of insulin. The molecular weight of the NDs, in addition to any adsorbed material, allows for the separation of components via centrifugation. Separation and analysis of remaining solutions yields supporting data concerning loading capacity and resultant release from the NDs. Fig. 5a illustrates protein adsorption of FITC insulin at a 5:1 ratio of NDs to insulin, demonstrating $89.8 \pm 8.5\%$ binding in water. ND–insulin and insulin samples were measured before and after centrifugation, resulting in lower insulin concentrations of the ND–insulin sample as compared to the insulin sample due to centrifugation.

A similar test was conducted using standard bovine insulin implementing the BCA protein assay. Adsorption of 25 μg/mL insulin to 100 μg/mL NDs (4:1 ratio of NDs to insulin) demonstrated $79.8 \pm 4.3\%$ binding, taking into account the pull-down effect of centrifugation on insulin. Fig. 5b shows the absorbance readouts for ND–insulin complexes before and after centrifugation, with the peak absorbance at 562 nm. The absorbance of the centrifuged sample is significantly lower than that of the initial sample.

Protein binding ratios were determined by calculating the difference in absorbance between initial and centrifuged samples, and subtracting the difference in initial and centrifuged insulin control. The insulin control must be taken into consideration due to the slight gradient formed when insulin is centrifuged.

3.4. Desorption

The desorption assays were conducted in a similar manner as the adsorption assays. Aqueous solutions of FITC-labeled and standard insulin were added to ND suspensions at 5:1 and 4:1 ratios, respectively. Initial and centrifuged samples were measured, and the amount of insulin desorbed was calculated. Comparing released FITC insulin at pH values of 8.90, 9.35, 10.35 and 11.53, maximum desorption was demonstrated at the most alkaline pH (Fig. 5c). Separate tests at pH 10.7 show the ND–insulin complex achieving $53.3 \pm 1.2\%$ desorption. Standard insulin release from the NDs at pH 7.1, 9.3 and 10.6 also showed that the greatest amount of elution occurred at a pH of 10.6 (Fig. 5d). This desorption profile shows that insulin release demonstrates proportionality to the pH of the solution. Separate tests conducted with the NDs and insulin at a 4:1 ratio in the presence of NaOH at pH 10.5 resulted in a $31.3 \pm 1.6\%$ release of insulin.

Fig. 6 illustrates the release of insulin from the NDs over a period of 5 days in NaOH (pH 10.5) and water. Cumulative insulin eluted was quantified by weight percentage of total adsorbed insulin. The

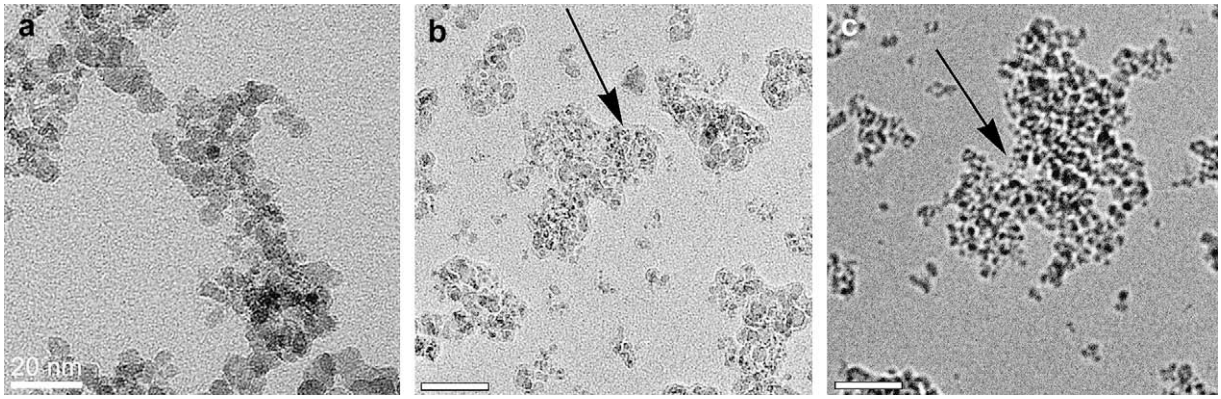

Fig. 2. TEM images of (a) bare NDs, (b) NDs with adsorbed insulin in aqueous solution and (c) NDs with adsorbed insulin after treatment with 1 mM NaOH adjusted to pH 10.5. There is an apparent layer or coating on the surface of NDs (b), as compared to bare NDs (a), with a thickness of approximately 5–10 nm. Seeing as the addition of insulin was the only difference in sample preparation between (a) and (b), the visible layer may indicate insulin adsorption. The material is not present on the NaOH-treated NDs (c). The scale bar represents 20 nm in (a) and 50 nm in (b, c).

amount of insulin released by day 1 from alkaline conditions (pH 10.5) was 32.7 ± 1.9 wt% compared to that of the water sample of 0.2 ± 0.1 wt%, revealing a considerable difference in release between the two samples. By day 3 both samples tended to plateau and release significantly less amounts of insulin, and by day 5 the total amount of insulin eluted by NaOH and water was 45.8 ± 3.8 wt% and 2.2 ± 1.2 wt%, respectively. These values denote more than 20 times the amount of insulin released from the samples containing NaOH than those containing water.

3.5. MTT cell viability assay

Cell viability tests under different insulin and ND conditions were performed (Fig. 7): DMEM (1), 0.1 μM insulin (2), 1 μM insulin (3), approximately 0.1 μM insulin released from ND–insulin complex by NaOH (pH 10.5) (4), resultant solution from centrifuged ND–insulin in water (5), ND–insulin treated with NaOH (1 μM total insulin) (6), NDs with bound insulin (ND–insulin, 1 μM total insulin) (7) and DMEM 10% FBS (8). Note that the amount of insulin adsorbed to the NDs for both ND-containing samples is equal to 1 μM in media if insulin completely dissociates from the ND surface. Significantly higher relative viability occurred from 0.1 μM (2) to 1 μM (3) concentrations of insulin, inferring increased viability at higher insulin concentrations. Relative viability for insulin released from the ND–insulin complexes by NaOH (4) is comparable to a relative viability between that of 0.1–1 μM insulin. Insulin desorbed by water (5) showed relative viability similar to that of 0.1 μM insulin, despite previous desorption results revealing insignificant levels of insulin in the resultant solution. ND–insulin treated with NaOH (6) demonstrated improved relative viability, greater than that of 1 μM insulin but less than 10% FBS media. ND–insulin (7) resulted in low relative cell viability comparable to DMEM and insulin released by water. For the ND–insulin treated with NaOH and ND–insulin conditions, NDs were present in the media during the recovery period allowing for cellular interactions with the NDs as compared to similar samples absent of NDs. Regular culture media, 10% FBS in DMEM (8), reflected the highest relative viability. An analysis of variance (ANOVA) statistical test was conducted yielding $P < 0.01$, indicating a significant difference among sample groups.

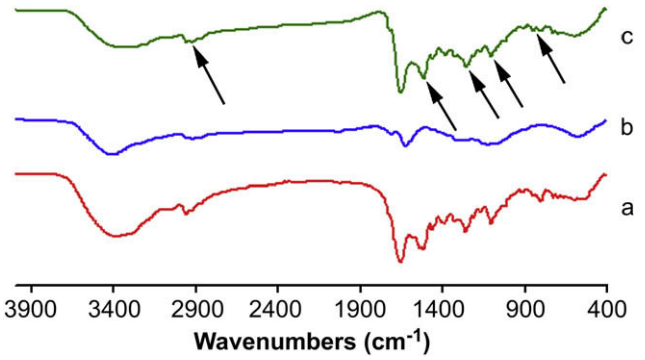

Fig. 3. Infrared spectra of (a) FITC insulin, (b) bare NDs and (c) ND–insulin complex. The arrows indicate the characteristic peaks of insulin present on the ND–insulin spectrum, as compared to the bare-ND spectrum. Image (c) suggests the formation of ND–insulin complexes as noted by the differential readouts. The data alludes to the non-covalent adsorption of insulin to NDs.

3.6. Quantitative RT-PCR

Pre-adipocyte differentiation yielded adipocytes by day 10 post-induction based on observations of morphology change and lipid vesicle formation in >90% of cells (Fig. 8). Pre-adipocytes (a) differ from adipocytes (b) by the clearly visible lipid vesicles. The effect of released insulin on adipocytes was quantified by RT-PCR for the genes Insulin 1 (Ins1) and Granulocyte colony-stimulating factor (Csf3/G-csf), and normalized to the housekeeping gene Ribosomal protein L32 (Rpl32). The relative expression of Ins1 in response to varying media solutions is shown (Fig. 9a). Compared to DMEM (1), insulin released by NaOH (3) and ND–insulin treated with NaOH (5) showed the highest relative expressions, indicating these conditions had the greatest effect on Ins1. Insulin released by water (4) and ND–insulin (6) resulted in moderate expression levels compared to the insulin-only condition (2) showing the

Table 1
DLS analysis of hydrodynamic nanoparticle cluster size and the associated polydispersity index (PDI) at pH7 and 10.5. NDs exhibited similar size and PDI at both pH conditions, while insulin at pH 10.5 tended to form larger particles with an increased PDI. Upon formation of the ND–insulin complex the PDI decreased, suggesting NDs mediate a relatively even distribution size of clusters.

	pH	Average size (μm)	PDI
Nanodiamond	7	1.67 ± 0.64	0.41 ± 0.084
	10.5	1.63 ± 0.66	0.30 ± 0.13
Insulin	7	1.59 ± 0.38	0.97 ± 0.046
	10.5	2.28 ± 0.66	0.99 ± 0.011
Nanodiamond–insulin	7	1.69 ± 0.37	0.23 ± 0.18
	10.5	1.05 ± 0.081	0.40 ± 0.12

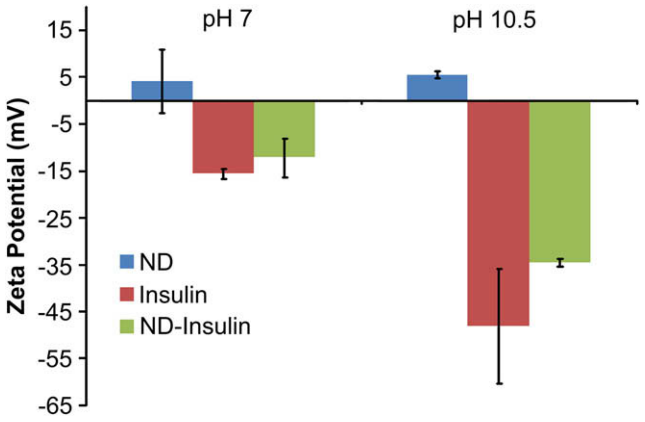

Fig. 4. Zeta potential changes associated with insulin and ND complexing at pH 7 and pH 10.5. NDs reveal a slightly positive zeta potential at both pH values, compared to the negative potential of insulin and the ND–insulin complex. The apparent difference in zeta potential between NDs and the ND–insulin complex implies an interaction between NDs and insulin.

lowest expression of Ins1. Csf3/G-csf relative expression is displayed in Fig. 9b and shows a similar trend as with Ins1 in that both insulin released by NaOH (3) and ND–insulin treated with NaOH (5) demonstrate high expression levels, while insulin released by water (4) and NDs with bound insulin (6) are significantly lower. The effect of 0.1 μM insulin on Csf3/G-csf, however, was comparably higher than that of Ins1. The ANOVA statistical test gave $P < 0.01$, indicating a significant difference among sample groups.

4. Discussion

4.1. Physical adsorption

Conditions during ND synthesis result in a functionalized carbon surface of hydroxyl and carboxyl groups, which can lead to a characteristic surface charge in aqueous solutions [8,33,34]. Such functional groups present favorable conditions for the physical adsorption of proteins via electrostatic interactions between surface elements such as anionic end groups ($-COO^-$) and the protonated amino groups ($-NH_3^+$) of polypeptides. In addition to charge–charge interactions, hydrogen bonds can form between $-NH_3^+$ and $-COO^-$ or other CO-containing surface groups, with H-bond binding energies between 10 and 30 kcal/mol [38,39,42]. Charged amino acid residues on the exterior of the insulin molecule contribute to its hydrophilicity and can be attracted to the ND surface. Although the isoelectric point of insulin is approximately 5.6 [43], indicating a slightly negative net charge at neutral pH, the electrostatic interactions and H-bonding between ND functional

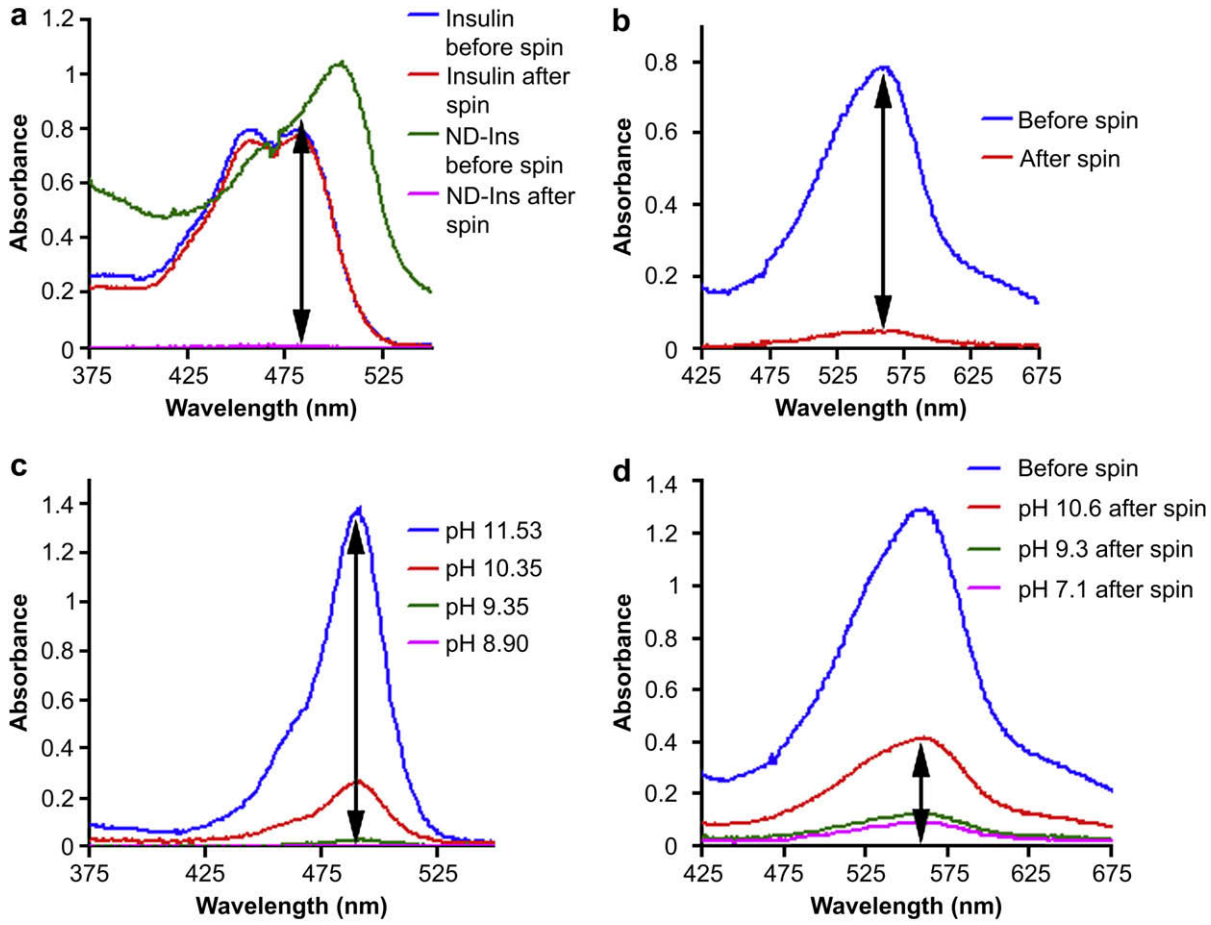

Fig. 5. UV/vis quantification of the adsorption and desorption of insulin from NDs. (a) Adsorption of FITC insulin to NDs is noted by the differential absorbance values attained between the initial and centrifuged ND–insulin, measured at 485 nm. (b) Absorbance of bovine insulin implementing the BCA protein assay, measured at 562 nm. (c) Desorption of FITC insulin from NDs in 1 mM NaOH adjusted to various pH values. Samples were centrifuged under alkaline conditions, and the resultant solution measured. (d) Desorption of bovine insulin from NDs using the BCA protein assay. From the release absorbance spectra, greater amounts of insulin are desorbed in alkaline environments, suggesting NaOH affects the charge characteristics of insulin.

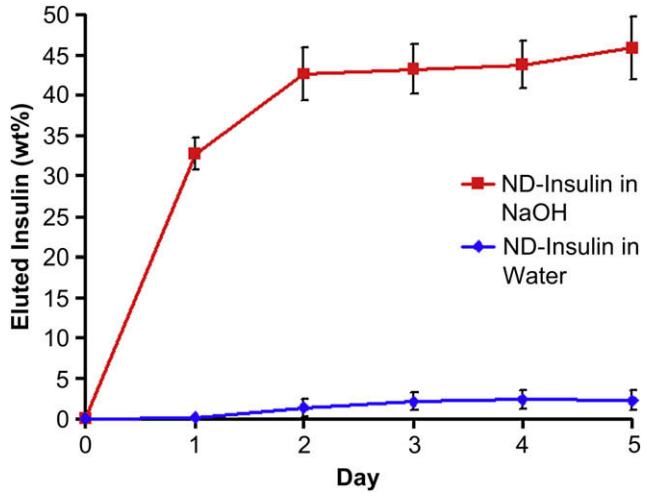

Fig. 6. Five-day insulin desorption test of ND–insulin samples treated with NaOH (pH 10.5) and water, showing insulin release in an alkaline pH environment. The cumulative weight percentage of released insulin was measured. The NaOH samples show increased desorption within the first 2 days and then a leveling-off of the amount released for a total desorption of 45.8 ± 3.8%. Samples treated with water, however, released only a fraction of insulin totaling 2.2 ± 1.2%. The majority of insulin released by NaOH occurred by day 1, indicating the alkaline solution had its maximal effect on fully-adsorbed NDs.

groups and biomolecules with amine groups may lead to attractive interactions. Fig. 1 illustrates this concept of insulin adsorption to the NDs in a neutral environment. As such, initial attempts to adsorb insulin onto the ND surface were completed and are supported by experimental data.

TEM imagery shows the NDs after immersion in aqueous insulin (Fig. 2b) with a visible layer of material coating the ND surface, as compared to bare NDs (a) Since the addition of insulin (b) is the only discriminating factor, it lends precedence to the material layer

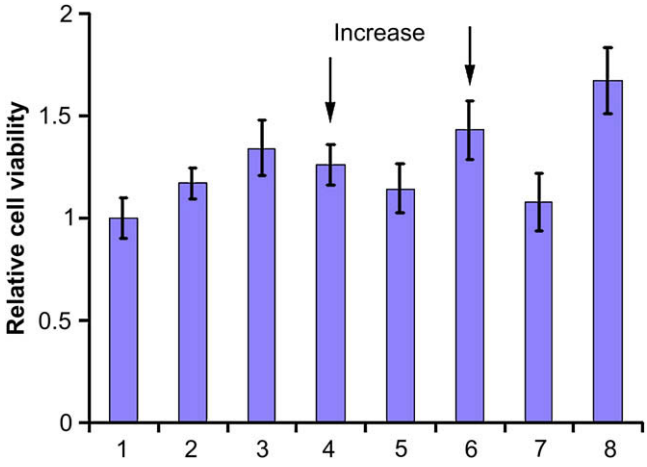

Fig. 7. MTT cell viability assay of RAW 264.7 macrophage cells under varying media conditions. Cells were serum-starved for 8 h, followed by a 24-hour recovery period with the indicated media solutions: (1) DMEM,(2) 0.1 μM insulin,(3) 1 μM insulin,(4) approximately 0.1 μM insulin released from ND–insulin by NaOH (pH 10.5),(5) resultant solution from centrifuged ND–insulin in water,(6) ND–insulin treated with NaOH (1 μM total insulin),(7) NDs with bound insulin (ND–insulin, 1 μM total insulin) and (8) DMEM 10% FBS. Relative viability of ND–insulin treated with NaOH (6) was similar to that of high insulin concentration (3) demonstrating effective recovery with the released insulin. Insulin released by NaOH (4) showed higher relative viability than that of insulin released by water (5), signifying a greater desorption via alkaline solutions. ANOVA statistical analysis gave $P < 0.01$, representing a significant difference among groups.

(thickness 5–10 nm) being identified as adsorbed insulin. The ND clusters seen in Fig. 2 boast very high surface areas allowing for substantial insulin adsorption to the ND surface. In fact, ND characterization has previously demonstrated a remarkable surface area of 450 m^2/g [9]. TEM imaging provides visual recognition of protein binding, and adsorption can be subsequently quantified by FT-IR spectroscopy. Insulin adsorption to the NDs is validated by FT-IR characterization of insulin, bare NDs and NDs with bound insulin (Fig. 3). The characteristic spectrum of insulin (a) is distinctly seen in the spectrum showing NDs with bound insulin (c) which serves as quantifiable results that would not be obtained otherwise from the NDs without adsorbed insulin (b). TEM imagery and FT-IR analysis thus provide additional evidence of insulin adsorption to the ND surface.

Further substantiation of the formation of ND–insulin complexes is given by UV/vis analysis. Adsorption tests revealed a 5:1 ratio of NDs to FITC insulin at optimal binding capacity (absence of excess insulin in resultant solution), demonstrating 89.8 ± 8.5% adsorption. Absence of measurable absorbance of the centrifuged ND–insulin sample (Fig. 5a) signifies considerable FITC insulin adsorption to the NDs. The absorbance difference at 485 nm between initial and centrifuged ND–insulin samples is attributed to the molecular weight of the NDs and settling of the NDs with bound insulin during centrifugation, leaving trivial amounts of residual insulin in solution. A slight difference between initial and centrifuged insulin control samples is used to normalize adsorption values since the molecular weight of insulin compared to the aqueous solution allows for the separation of components. Fig. 5a reveals an altered absorbance readout for ND–insulin when compared to that of insulin, with absorbance peaks of insulin and ND–insulin shifting from 485 nm to 505 nm. This peak shift is possibly due to a change in optical properties of the FITC molecule when FITC-labeled insulin adsorbs to the NDs, indicating a possible conformational change in protein structure often observed in protein adsorption [44].

Similar results were obtained from standard bovine insulin adsorption tests with an optimal ND-to-insulin binding ratio of 4:1. A higher adsorption ratio for standard bovine insulin is expected given that the molecular weight of insulin as compared to that of FITC-labeled insulin. Fig. 5b depicts BCA protein assay absorbance measurements revealing contrasting peaks for initial and centrifuged ND–insulin samples associating to a substantial 79.8 ± 4.3% insulin adsorption.

Insulin adsorption tests involving FITC-labeled and standard insulin are consistent with previous investigations verifying protein–ND binding [39] and exhibit exceptional adsorption capabilities, with approximately 80% of insulin binding to the ND surface at optimal ND–insulin ratios. The protein loading capacity of the NDs as demonstrated by the adsorption tests imply a relatively efficient drug-loading process where the majority of available protein is adsorbed to the ND surface. The facile method of physical adsorption in aqueous solutions is ideal for drug delivery preparation methods by eliminating complex conjugation protocols that can affect the properties of the drug or substrate.

The physical interaction between the NDs and insulin was also characterized via dynamic light scattering (Table 1). NDs formed clusters of similar hydrodynamic size and distribution at pH 7 and 10.5 while insulin aggregation was also observed and has been investigated in additional studies [45–47]. Upon insulin complexing with the NDs, the polydispersity index is not only reduced, but the zeta potential of the clusters is also altered to a negative value (Fig. 4). The reduction of PDI as seen with the formation of ND–insulin complexes, compared to that of insulin, indicates the ND-mediated development of a more uniform nanomaterial–protein complex. NDs originally maintained a slightly positive zeta potential within alkaline solutions while insulin inherently possessed

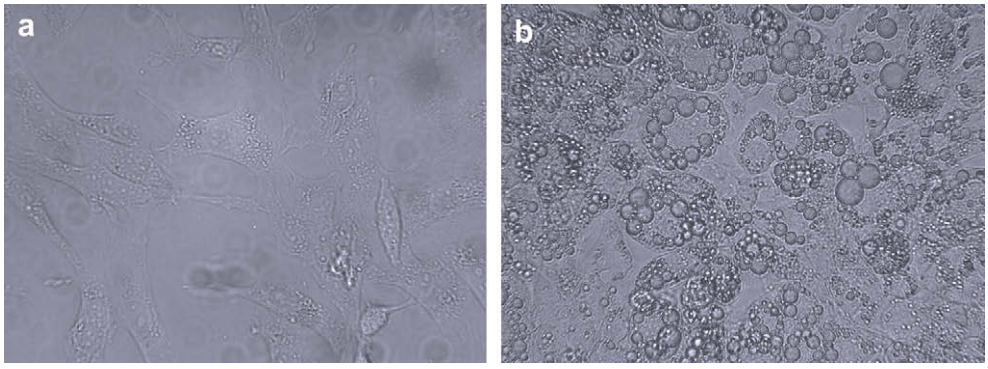

Fig. 8. (a) 3T3-L1 pre-adipocytes and (b) differentiated adipocytes, showing a clear difference in morphology between the two cell types. The pre-adipocyte fibroblast cells undergo differentiation upon supplementing media with insulin, dexamethasone and IBMX, becoming fully differentiated by day 10 post-induction. Lipid vesicle formation occurs during differentiation and can be seen in (b). 250× magnification.

a negative zeta potential that further decreased in alkaline solutions. This zeta potential was retained upon introduction to the NDs, implying insulin adherence onto the ND surface. This result is further verified since the cluster's zeta potential at pH 10.5 lies within a narrow confined range of values. The clear difference in relative zeta potential between bare NDs and ND-insulin suggests an interaction between the NDs and insulin.

4.2. pH-mediated desorption

Release of insulin from the ND–insulin complex was observed in alkaline sodium hydroxide solutions and can be explained by a change in charge characteristics affected by pH modification. Insulin in aqueous environments at a pH above the isoelectric point may carry a negative net surface charge owing to the charge alteration of the functional end groups. Subsequently, the negative charge can become stronger with increased alkalinity and affect charge interactions with other species. Thus, the effect of pH on desorption is rather straightforward. Insulin molecules bound to charged functional groups on the ND surface via electrostatic interactions and hydrogen bonding will begin to display altered charge characteristics as the aqueous environment shifts from neutral to alkaline, and therefore release from the NDs by mechanisms such as electrostatic repulsion.

The amount of desorbed insulin seems to be proportional to the pH of the solution, showing increased insulin release in alkaline solutions (Fig. 5c–d). The absorbance spectrum of FITC-labeled insulin desorption (Fig. 5c) represents an increase in desorption as the pH shifts from 8.90 to 11.53, and a similar pattern is expressed in Fig. 5d with standard insulin. These results are consistent with the pH-dependent desorption premise mentioned previously. The $31.3 \pm 1.6\%$ desorption of standard insulin in NaOH demonstrates that insulin is capable of being adsorbed as well as subsequently released from the ND surface into an aqueous medium.

Many practical applications necessitate the release of a drug over time, and in order to quantify the timed-release of insulin, a 5-day desorption test was conducted using the NDs with bound insulin in both NaOH and water. The disproportion between the two release curves in Fig. 6 exemplifies the difference in desorption ability of alkaline and neutral solutions. Alkaline-mediated desorption reached $45.8 \pm 3.8\%$ by day 5 compared to only $2.2 \pm 1.2\%$ in water. The bulk of the desorption occurred by day 1 of the test, suggesting a burst release of insulin from the NDs. Day 2, however, did produce a moderate insulin release. The time-dependency of insulin release enables the ND–insulin complex to release insulin in a sustained fashion upon exposure to alkaline environments.

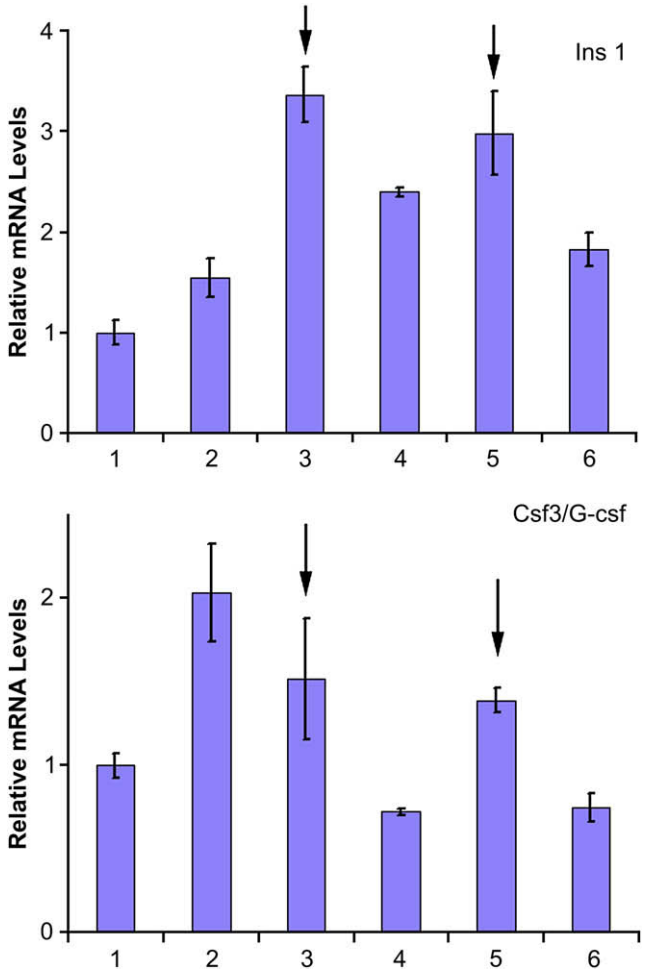

Fig. 9. Real-time PCR gene expression for Ins1 and Csf3/G-csf under media conditions. 3T3-L1 adipocytes were serum-starved for 4 h prior to a 2-hour recovery period in different media solutions: (1) DMEM, (2) 0.1 μM insulin, (3) 0.1 μM insulin released from ND–insulin by NaOH (pH 10.5), (4) resultant solution from centrifuged ND–insulin in water, (5) ND–insulin treated with NaOH (1 μM total insulin) and (6) NDs with bound insulin (ND–insulin, 1 μM total insulin). Both genes showed increased expression for insulin released by NaOH (3) and ND–insulin treated with NaOH (5), indicating effective insulin release by alkaline conditions while preserving activity. Comparatively, insulin released by water (4) and ND–insulin (6) demonstrated low relative expression for both genes alluding to the sequestration of insulin to the ND surface preventing protein function. Gene expression plot representative of RT-PCR samples. ANOVA: $P < 0.01$.

4.3. Preservation of protein function

Results discussed in the previous section establish a basis for pH-mediated insulin desorption, yet practical use of such a system relies on the retained function of the drug upon release from the ND surface. The data obtained from MTT viability assays and RT-PCR suggest insulin function is indeed preserved subsequent to desorption as noted by cell viability and gene expression analysis. Furthermore, insulin sequestered on the ND surface seems to remain inactive to cellular pathways despite the presence of the ND–insulin complex.

Cell viability data (Fig. 7) reveal an increase in cellular recovery with insulin released from the NDs by NaOH and ND–insulin complexes treated with NaOH, with the latter being comprised of the NDs and desorbed insulin in media solution. The increased viability levels of cells in these two media conditions, as compared to the DMEM baseline, signify that the released insulin is activating cellular recovery pathways following the starvation period. Also, viability of ND–insulin treated with NaOH indicates cellular recovery occurs in the presence of the released insulin and the subsequent NaOH-treated NDs which may or may not result in bare ND surfaces. Previous investigations implementing serum-starvation and insulin recovery on RAW 264.7 macrophages [48] are consistent with the acquired MTT data showing insulin-mediated recovery.

Insulin released by water and ND–insulin, in contrast, yielded low viability levels, implying little or no insulin release in the neutral environment. The ND–insulin complex seems to prevent the adsorbed insulin from impacting cellular pathways even with insulin exposed on the ND surface. Proteins are often known to undergo a conformational change when adsorbed to a surface [44] leading to altered physical properties, and insulin sequestering onto the ND surface may prevent the activation of cellular pathways. Effective isolation of insulin from a soluble environment until mediation by alkalinity is an important component towards the enhanced specificity of insulin delivery using this system.

Gene expression studies from RT-PCR closely correlated with results from the MTT viability assays. Fig. 9 shows the relative expression of genes Ins1 and Csf3/G-csf, which are upregulated by insulin stimulation of adipocyte cells [40]. Expression levels for samples containing insulin released by NaOH and ND–insulin treated with NaOH increased for each gene, demonstrating the effectiveness of insulin after desorption from the ND surface. Absence of active insulin does not increase expression levels as noted by the DMEM baseline. Similar to the MTT results, the insulin released by water and ND–insulin show reduced expression levels for each gene, indicating insufficient response to reduced insulin concentration so as to activate cellular pathways. This suggests protein activity is retained for insulin desorbed from the NDs as determined by genetic expression attributed to insulin stimulation. Additionally, adsorbed insulin, despite being bound to the ND surface, does not increase cell viability or gene expression. In this manner the ND–insulin complex presents a unique approach for insulin delivery with improved specificity in alkaline environments while remaining stable in neutral solutions.

These findings also suggest insulin adsorption and elution from the NDs is pH-dependent, an observation that can be scaled up for therapeutic purposes. Insulin desorption is shown to increase in alkaline environments possibly by the action of a change in surface charge of the protein, thereby decreasing the propensity of ND-to-insulin attraction. Exploiting this pH-mediated desorption mechanism may provide unique advantages for enhanced drug delivery methods. It is well understood that insulin accelerates wound healing by acting as a growth hormone [49–53]. Furthermore, previous investigations have confirmed an increase in alkalinity of wound tissue due to bacterial colonization, sometimes at levels as high as pH 10.5 [54,55]. Considering these two observations the ND–insulin complex may serve as a useful therapeutic drug delivery system for the treatment of wound healing. Administration of the NDs with adsorbed insulin may be able to accelerate the healing process and decrease the incidence of infection by releasing insulin in alkaline wound areas. Systemic activation of insulin would be limited as the release of insulin would occur at the site of injury. These studies and our current findings offer the potential of applying an ND-based insulin release mechanism with enhanced specificity as a therapeutic strategy towards wound healing.

5. Conclusion

In this study we have demonstrated the efficient, non-covalent adsorption of insulin to the NDs by means of physical adsorption and investigated the pH-dependency of protein desorption. Exposure of the ND–insulin complex to alkaline environments mediates the interaction between the NDs and insulin resulting in protein release. Imaging methods and adsorption/desorption assays reveal effective binding of insulin to the NDs and significant insulin release under alkaline conditions. MTT and RT-PCR analysis indicate preserved function following desorption, while adsorbed insulin remained largely inactive. As a result, NDs may serve as a proficient platform for insulin delivery and show promise for a wide range of therapeutic treatments.

Acknowledgements

D.H. gratefully acknowledges support from a National Science Foundation CAREER Award (CMMI-0846323), National Science Foundation Mechanics of Materials program grant (CMMI-0856492), V Foundation for Cancer Research V Scholars Award, National Science Foundation Center for Scalable and Integrated NanoManufacturing (SINAM) grant DMI-0327077, Wallace H. Coulter Foundation Early Career Award in Translational Research, National Science Foundation National Center for Learning & Teaching in Nanoscale Science and Engineering (NCLT), and National Institutes of Health grant U54 A1065359. R.L. acknowledges support from a Northwestern University Ryan Fellowship.

Appendix

Figures with essential colour discrimination. The majority of the figures in this article are difficult to interpret in black and white. The full colour version can be found in the on-line version, at doi:10.1016/j.biomaterials.2009.07.004.

References

[1] Mochalin VN, Gogotsi Y. Wet chemistry route to hydrophobic blue fluorescent nanodiamond. J Am Chem Soc 2009;13:4594–5.
[2] Chang YR, Lee HY, Chen K, Chang CC, Tsai DS, Fu CC, et al. Mass production and dynamic imaging of fluorescent nanodiamonds. Nat Nanotechnol 2008;3:284–8.
[3] Fu CC, Lee HY, Chen K, Lim TS, Wu HY, Lin PK, et al. Characterization and application of single fluorescent nanodiamonds as cellular biomarkers. Proc Natl Acad Sci U S A 2007;104:727–32.
[4] Deming TJ. Methodologies for preparation of synthetic block copolypeptides: materials with future promise in drug delivery. Adv Drug Deliv Rev 2002;54:1145–55.
[5] Zhang L, Chan JM, Gu FX, Rhee JW, Wang AZ, Radovic-Moreno AF, et al. Self-assembled lipid–polymer hybrid nanoparticles: a robust drug delivery platform. ACS Nano 2008;2:1696–702.
[6] Farokhzad OC, Langer R. Impact of nanotechnology on drug delivery. ACS Nano 2009;3:16–20.
[7] Xu P, Gullotti E, Tong L, Highley CB, Errabelli DR, Hasan T, et al. Intracellular drug delivery by poly(lactic-co-glycolic acid) nanoparticles, revisited. Mol Pharmacol 2009;6:190–201.
[8] Huang H, Pierstorff E, Osawa E, Ho D. Active nanodiamond hydrogels for chemotherapeutic delivery. Nano Lett 2007;7:3305–14.

[9] Lam R, Chen M, Pierstorff E, Huang H, Osawa E, Ho D. Nanodiamond-embedded microfilm devices for localized chemotherapeutic elution. ACS Nano 2008;2:2095–102.
[10] Hauck TS, Jennings TL, Yatsenko T, Kumaradas JC, Chan WCW. Enhancing the toxicity of cancer chemotherapeutics with gold nanorod hyperthermia. Adv Mater 2008;20:3832–8.
[11] Cheong SJ, Lee CM, Kim SL, Jeong HJ, Kim EM, Park EH, et al. Superparamagnetic iron oxide nanoparticles-loaded chitosan–linoleic acid nanoparticles as an effective hepatocyte-targeted gene delivery system. Int J Pharm 2009;372:169–76.
[12] Dobson J. Gene therapy progress and prospects: magnetic nanoparticle-based gene delivery. Gene Ther 2006;13:283–7.
[13] Panyam J, Labhasetwar V. Biodegradable nanoparticles for drug and gene delivery to cells and tissue. Adv Drug Deliv Rev 2003;55:329–47.
[14] Allen TM, Cullis PR. Drug delivery systems: entering the mainstream. Science 2004;303:1818–22.
[15] Gwinn MR, Vallyathan V. Nanoparticles: health effects – pros and cons. Environ Health Perspect 2006;114:1818–25.
[16] Niemeyer CM. Nanoparticles, proteins, and nucleic acids: biotechnology meets material science. Angew Chem Int Ed 2001;40:4128–58.
[17] Gelperina S, Kisich K, Iseman MD, Heifets L. The potential advantages of nanoparticle drug delivery systems in chemotherapy of tuberculosis. Am J Respir Crit Care 2005;172:1487–90.
[18] Hilder TA, Hill JM. Carbon nanotubes as drug delivery nanocapsules. Curr Appl Phys 2007;8:258–61.
[19] Ajima K, Yudasaka M, Murakami T, Maigné A, Shiba K, Iijima S. Carbon nanohorns as anticancer drug carriers. Mol Pharm 2005;2:475–80.
[20] Cevc G, Richardsen H. Lipid vesicles and membrane fusion. Adv Drug Deliv Rev 1999;38:207–32.
[21] Mirsa RDK. Magnetic nanoparticle carrier for targeted drug delivery: perspective, outlook and design. J Mater Sci Technol 2008;24:1011–9.
[22] Huang H, Chen M, Bruno P, Lam R, Robinson E, Gruen D, et al. Ultra-nanocrystalline diamond thin films functionalized with therapeutically active collagen networks. J Phys Chem B 2009;113:2966–71.
[23] Behler KD, Stravato A, Mochalin V, Korneva G, Yushin G, Gogotsi Y. Nanodiamond–polymer composite fibers and coatings. ACS Nano 2009;3:363–9.
[24] Hanson JA, Chang CB, Graves SM, Li Z, Mason TG, Deming TJ. Nanoscale double emulsions by single-component block copolypeptides. Nature 2008;455:85–8.
[25] Auguste DT, Furman K, Wong A, Fuller J, Armes SP, Deming TJ, et al. Triggered release of siRNA from poly(ethylene glycol)-protected, pH-dependent liposomes. J Control Release 2008;130:266–74.
[26] Yeo Y, Ito T, Bellas E, Highley CB, Marini R, Kohane DS. In situ cross-linkable hyaluronan hydrogels containing polymeric nanoparticles for preventing postsurgical adhesions. Ann Surg 2007;245:819–24.
[27] Pathak P, Meziani MJ, Desai T, Sun YP. Nanosizing drug particles in supercritical fluid processing. J Am Chem Soc 2004;126:10842–3.
[28] Joshi JM, Bhumkar DR, Joshi K, Pokharkar V, Sastry M. Gold nanoparticles as carriers for efficient transmucosal insulin delivery. Langmuir 2005;22:300–5.
[29] LaVan DA, McGuire T, Langer R. Small-scale systems for in vivo drug delivery. Nature 2003;21:1184–91.
[30] Kim BS, Oh JM, Hyun H, Kim KS, Lee SH, Kim YH, et al. Insulin-loaded microparticles for in vivo delivery. Mol Pharm 2009;6:353–65.
[31] Sarmento B, Ribeiro A, Veiga F, Ferreira D, Neufeld R. Oral bioavailability of insulin contained in polysaccharide nanoparticles. Biomacromolecules 2007;8:3054–60.
[32] Wood KM, Stone GM, Peppas NA. Wheat germ agglutinin functionalized complexation hydrogels for oral insulin delivery. Biomacromolecules 2008;9:1293–8.
[33] Huang H, Pierstorff E, Osawa E, Ho D. Protein-mediated assembly of nanodiamond hydrogels into a biocompatible and biofunctional multilayer nanofilm. ACS Nano 2008;2:203–12.
[34] Yeap WS, Chen S, Loh KP. Detonation nanodiamond: an organic platform for the suzuki coupling of organic molecules. Langmuir 2009;25:185–91.
[35] Panessa-Warren BJ, Warren JB, Wong SS, Misewich JA. Biological cellular response to carbon nanoparticle toxicity. J Phys Condens Matter 2006;18:S2185–201.
[36] Puzyr AP, Baron AV, Purtov KV, Bortnikov EV, Skobelev NN, Mogilnaya OA, et al. Nanodiamonds with novel properties: a biological study. Diamond Relat Mater 2007;16:2124–8.
[37] Schrand AM, Huang H, Carlson C, Schlager JJ, Osawa E, Hussain SM, et al. Are diamond nanoparticles cytotoxic? J Phys Chem B 2007;111:2–7.
[38] Zhao W, Xu JJ, Qiu QQ, Chen HY. Nanocrystalline diamond modified gold electrode for glucose biosensing. Biosens Bioelectron 2006;22:649–55.
[39] Huang LCL, Chang HC. Adsorption and immobilization of cytochrome c on nanodiamonds. Langmuir 2004;20:5879–84.
[40] Cao H, Urban JF, Anderson RA. Insulin increases tristetraprolin and decreases VEGF gene expression in mouse 3T3-L1 adipocytes. Obesity 2008;16:1208–18.
[41] Adochio R, Leitner JW, Hedlund R, Draznin B. Rescuing 3T3-L1 adipocytes from insulin resistance induced by stimulation of Akt-mammalian target of rapamycin/p70 S6 kinase (S6K1) pathway and serine phosphorylation of insulin receptor substrate-1: effect of reduced expression of p85α subunit of phosphatidylinositol 3-kinase and S6K1 kinase. Endocrinology 2009;150:1165–73.
[42] Speller CV, Meot-Ner M. The ionic hydrogen bond and ion solvation. 3. Bonds involving cyanides. Correlations with proton affinities. J Phys Chem 1985;89:5217–22.
[43] Farías RN, Viñals AEL, Posse E, Morero RD. Relationship between isoelectric point of native and chemically modified insulin and liposomal fusion. Biochem J 1989;264:285–7.
[44] Feng L, Andrade JD. Protein adsorption of low-temperature isotropic carbon: I. Protein conformational change probed by differential scanning calorimetry. J Biomed Mater Res 1994;28:735–43.
[45] Sajeesh S, Sharma CP. Cyclodextrin–insulin complex encapsulated polymethacrylic acid based nanoparticles for oral insulin delivery. Int J Pharm 2006;325:147–54.
[46] Tokumoto S, Higo N, Sugibayashi K. Effect of electroporation and pH on the iontophoretic transdermal delivery of human insulin. Int J Pharm 2006;326:13–9.
[47] Constantino HR, Langer R, Klibanov AM. Moisture-induced aggregation of lyophilized insulin. Pharm Res 1994;11:21–9.
[48] Iida KT, Suzuki H, Sone H, Shimano H, Toyoshima H, Yatoh S, et al. Insulin inhibits apoptosis of macrophage cell like, THP-1 cells, via phosphatidylinositol-3-kinase-dependent pathway. Arterioscler Thromb Vasc Biol 2002;22:380–6.
[49] Greenway SE, Filler LE, Greenway FL. Topical insulin in wound healing: a randomised, double-blind, placebo-controlled trial. J Wound Care 1999;8:526–8.
[50] Liu Y, Petreaca M, Yao M, Martins-Green M. Cell and molecular mechanisms of keratinocyte function stimulated by insulin during wound healing. BMC Cell Biol 2009;10:1–15.
[51] Pierre EJ, Barrow RE, Hawkins HK, Nguyen TT, Sakurai Y, Desai M, et al. Effects of insulin on wound healing. J Trauma 1998;44:342–5.
[52] Liu Y, Zhang X, Zhang Z, Fang PY, Xu WS. Effects of topical application of insulin on the wound healing in scalded rats. Chin J Burns 2004;20:98–101.
[53] Zhang XJ, Wu X, Wolf SE, Hawkins HK, Chinkes DL, Wolfe RR. Local insulin–zinc injection accelerates skin donor site wound healing. J Surg Res 2007;142:90–6.
[54] Schneider LA, Korber A, Grabbe S, Dissemond J. Influence of pH on wound-healing: a new perspective for wound-therapy? Arch Dermatol Res 2007;298:413–20.
[55] Osti E. Skin pH variations from the acute phase to re-epithelialization in burn patients treated with new materials (Burnshield, semipermeable adhesive film, Dermasilk, and Hyalomatrix). Non-invasive preliminary experimental clinical trial. Ann Burns Fire Disasters 2007;21(2):73–7.